Polymer 53 (2012) 4631–4636

Contents lists available at SciVerse ScienceDirect

Polymer

journal homepage: www.elsevier.com/locate/polymer

Directed inorganic modification of bi-component polymer fibers by selective vapor reaction and atomic layer deposition

Bo Gong, Joseph C. Spagnola, Sara A. Arvidson, Saad A. Khan, Gregory N. Parsons*

Department of Chemical and Biomolecular Engineering, North Carolina State University, Raleigh, NC 27695, USA

ARTICLE INFO

Article history:
Received 5 May 2012
Received in revised form
28 July 2012
Accepted 8 August 2012
Available online 21 August 2012

Keywords:
Atomic layer deposition
Bi-component fibers
Vapor infiltration

ABSTRACT

Nanocomposite organic/inorganic materials with spatially-controlled composition can be formed using vapor-phase atomic layer deposition (ALD) on bi-component polymer fibers. The ALD process promotes selective precursor infusion into the inner core of a core/shell polymer fiber, yielding nanoparticles encapsulated within the core. Likewise, choosing alternate precursors or reaction conditions yield particles or films on the outer polymer shell. In-situ infrared spectroscopy and transmission electron microscopy show that infusion yields selective dispersion of aluminum oxide in different polymer regions, forming fine nanoparticle dispersions or films. Selective inclusion of metal oxide materials during atomic layer deposition on polymers can create unique organic/inorganic composite structures for many advanced uses.

1. Introduction

Nanocomposite materials composed of an organic host with inorganic inclusions show unique prospects for use in drug delivery [1,2], chemical separation [3–5] and energy conversion and storage systems [6–10]. Polymer-based composites can retain the inherent mechanical properties and flexibility of the organic while also showing improved thermal, optical and electrical performance due to the added inorganic component [11–15]. Conventional solution-based synthesis methods typically require mechanical mixing of organic and inorganic precursors, and for the most part, result in inorganic clusters or particles distributed within the organic structure [16–18]. However, the ability to tune nanocomposite structure and component distribution will further extend applications. New means to prepare hybrid materials with desired local composition continue to attract research interest [19,20].

Exposing polymers to vapor-phase inorganic atomic layer deposition (ALD) reactions can result in sub-surface metal oxide nucleation and particle growth. The particles are dispersed generally near the substrate surface, but the reaction depth depends strongly on the substrate and the specific reaction chemistry [21–23]. Because metal organic precursor reactivity varies with polymer species, multicomponent systems can be designed such that selective reaction occurs only in certain phases to enable preparation of hybrid materials with localized functionalities [23,24].

In this paper, we demonstrate selective reaction between metal organic vapor and polymers in a multi-component polymer structure. We used two types of bi-component core/sheath fibers, approximately 12–15 μm in total diameter. One fiber type consisted of a ~7–8 μm core of polylactic acid (PLA) surrounded by a ~2–3 μm thick polypropylene (PP) sheath (referred to as PLA/PP fibers), while the other fiber type featured the reverse configuration with PP in the core (i.e., PP/PLA fibers). The PP and PLA materials were selected because of their distinctively different reactivity. PP is well known as a chemically stable polymer. However, PLA has groups known to react with metal organic vapors during ALD process [25]. Moreover, the PP and PLA have similar melting points [26] which help the processing of core-sheath bi-component polymer fibers. We exposed both types of fibers to an aluminum oxide atomic layer deposition sequence using trimethylaluminum (TMA) and water. The TMA diffuses into both polymers and forms well-defined inorganic inclusions. However, the location and structure (i.e., continuous film or isolated particles) of the inorganic component is controlled by the fiber structure and ALD deposition and exposure conditions. In this manner, the vapor-phase ALD process enables fine control of inorganic material integration with polymer matrices for advanced nanocomposite synthesis.

2. Experimental procedures

2.1. Materials

Poly(lactic acid) resin for fiber spinning was provided by NatureWorks® LLC, Minnetonka, MN (product 6202D, weight-

* Corresponding author.
E-mail address: parsons@ncsu.edu (G.N. Parsons).

0032-3861/$ – see front matter © 2012 Elsevier Ltd. All rights reserved.
http://dx.doi.org/10.1016/j.polymer.2012.08.018

average molecular weight (M_W) approximately 97,000 Da) [26,27] and poly(lactic acid) for preparing films was purchased from Aldrich (reported M_W 60,000 Da). Polypropylene was supplied by Sunoco Chemicals Polymers Division, Pittsburg, PA (product CP360H, M_W 178,000 Da reported by manufacturer). Decahydronaphthalene ($C_{10}H_{18}$, 99% anhydrous) and chloroform ($CHCl_3$, 99% anhydrous) were obtained from Aldrich and used as received. For atomic layer deposition, trimethylaluminum (TMA, 98%) was purchased from Strem Chemicals, and ultra-high purity argon (Ar, 99.999%, National Welders Supply Co.) was used as the purge and carrier gas.

2.2. Polymer film and fiber preparation

Polypropylene fibers were dissolved in decahydronaphthalene at 60 °C (1 wt%), passed through a syringe filter (polyvinylidene fluoride, 0.22 μm pore size, Fisher Scientific) and drop cast on a silicon substrate to produce a film. Once several drops of the solution were placed on the Si wafer, the wafer was spun at 6000 rpm for 60 s. The resultant PP film on Si was ~1.3 μm thick. PLA was dissolved in chloroform at room temperature, and a similar procedure was employed to fabricate the PLA film [23]. Core/sheath PP/PLA and PLA/PP fibers were melt spun at the Nonwovens Cooperative Research Center (NCRC) Partners' Pilot Spunbond line located at North Carolina State University as previously described [26].

2.3. Atomic layer deposition

Atomic layer deposition of Al_2O_3 and TMA/water vapor phase infiltration were performed at constant temperature of 120 °C at an operating pressure of ~1 Torr in a homemade hot wall reactor described previously [28,29]. Ultra-high purity argon was further purified by an inert gas filter (Aeronex GateKeeper, Entegris) before entering the reactor.

The temperature of 120 °C was chosen based on the thermal properties of the polymer substrates and the requirements for ALD process. PLA and PP have melting points of 155–165 °C [26] which limit the process temperature. On the other hand, the temperature needs to be high enough to activate the chemical reaction. Moreover, this process temperature is higher than the Tg of the polymers (~0 and 60 °C respectively for PP [30] and PLA [31]), which could allow metal organic vapors diffuse into the polymer substrates more easily.

In a typical ALD cycle, TMA flowed into the reactor for 1 s followed by 60 s of argon gas purge. This was followed by a 1 s water dose and another 60 s Ar purge. This ALD sequence is referred to as a "short cycle" and was repeated multiple times to form a conformal coating or "film" of alumina oxide. For some runs, we used a much longer precursor exposure sequence, which we refer to as a "long cycle" or more generally as "sequential vapor infiltration." For one long cycle, we flow TMA for 5 s then isolate the chamber for an additional 60 s, resulting in an overall 65 s exposure. We then purge for 60 s, and repeat the 65 s flow/exposure step for water and the 60 s purge. Previous results show that the ALD precursors can diffuse deep into the surface of some polymers, and these long exposure times will promote more diffusion into the more porous or less reactive polymers.

For in-situ FTIR experiments, we mounted the planar, polymer films on silicon wafers in another ALD reactor described previous in detail [25,29]. This reactor allowed the IR beam to pass through the polymer, and data was collected during the argon exposure step after TMA exposure, and then again after the water exposure step. For these tests, the sample was exposed to TMA for 5 s, followed by chamber isolation for 60 s, and an argon purge for 280 s. The IR data was collected for ~150 s during the 280 s Ar purge step. This subcycle was then repeated for the water exposure step, and the overall cycle was repeated a few times for each polymer. The substrate temperature was held at 80 °C for all the IR experiments. Using the previously collected spectrum as the background, changes in IR modes provide information on the specific reaction mechanisms as well as the extent of precursor reactivity [25].

2.4. Materials characterization

The morphology of TMA/water treated core/sheath fiber mat samples was determined by scanning electron microscopy (SEM) and transmission electron microscopy (TEM). An FEI PHENOM bench-top scanning electron microscope was used to collect relatively low magnification SEM images. A Hitachi HF 2000 transmittance electron microscope operated at 200 kV was used for TEM imaging. For TEM imaging, fibers were first embedded in Spurr low-viscosity epoxy resin (Ladd Research Industries). After curing overnight at room temperature, the resin was then cut into thin layer (~70 nm) using a Lecia Ultracut diamond knife microtome. The thin layers were then transferred on Cu mesh grids for TEM imaging. For higher magnification SEM imaging, a Hitachi S3200 SEM was also used to image the cross section of the bi-component fiber using in the microtomed slices. An Oxford Isis Energy-dispersive X-ray spectroscopy (EDS) system is also attached to the instrument which allows for elemental analysis. Before imaging, samples were loaded into a bench top sputter coater, and a 5 nm layer of gold/platinum was coated on to the sample. Each EDS scan line consisted of 200 points with 10 s collecting time for each point.

X-ray photoelectron spectroscopy (XPS) was performed in with a Kratos AXIS Ultra spectrometer equipped with an aluminum source and spherical mirror analyzer. Thin films of PP and PLA on silicon, approximately 1 cm × 1 cm were used for XPS experiments. Survey spectra were obtained from 1200 to 0 eV with 1 eV steps and a dwell time of 0.2 s. Atomic percentages were calculated using the survey scans and the CasaXPS software package. Detail C 1s scans were also performed on the same samples.

3. Results and discussion

We exposed both PLA/PP and PP/PLA core/sheath fibers to 100 short ALD cycles at 120 °C then imaged the samples under SEM. The results are in Fig. 1. After ALD, the PLA/PP core/sheath fiber retains its original morphology, with no significant visible change. However, the result is very different for the PP/PLA core/sheath fiber. The PLA sheath reacted heavily during the TMA/water process, but the PP core remains intact. This is consistent with a much higher extent of reaction for TMA with PLA compared to TMA with PP [25].

To characterize the precursor reaction, we performed in-situ FTIR analysis of TMA and water reaction with planar PP and PLA films. Results in Fig. 2a show IR data collected during TMA/water exposure to PLA. The bottom spectrum is collected from the PLA, showing characteristic peaks for the ester groups (C═O stretching at 1751 cm^{-1} and C–O stretching at 1188 cm^{-1}). The figure also shows differential spectra after the first TMA, first water, second TMA and second water exposure steps. After the first TMA exposure, we note an increase of the asymmetric and symmetric C–H stretching modes, ν_a (CH_3) and ν_s (CH_3) at 2939 and 2898 cm^{-1} respectively, ascribed to reaction of TMA with the polymer. The increase at about 1600 cm^{-1} is assigned to O–C–O stretching corresponding to the formation of aluminum carbonate groups [32,33]. Almost all the absorbance related to ester groups is removed upon TMA exposure, suggesting the strong interaction between TMA and the ester groups on PLA polymer chain promote

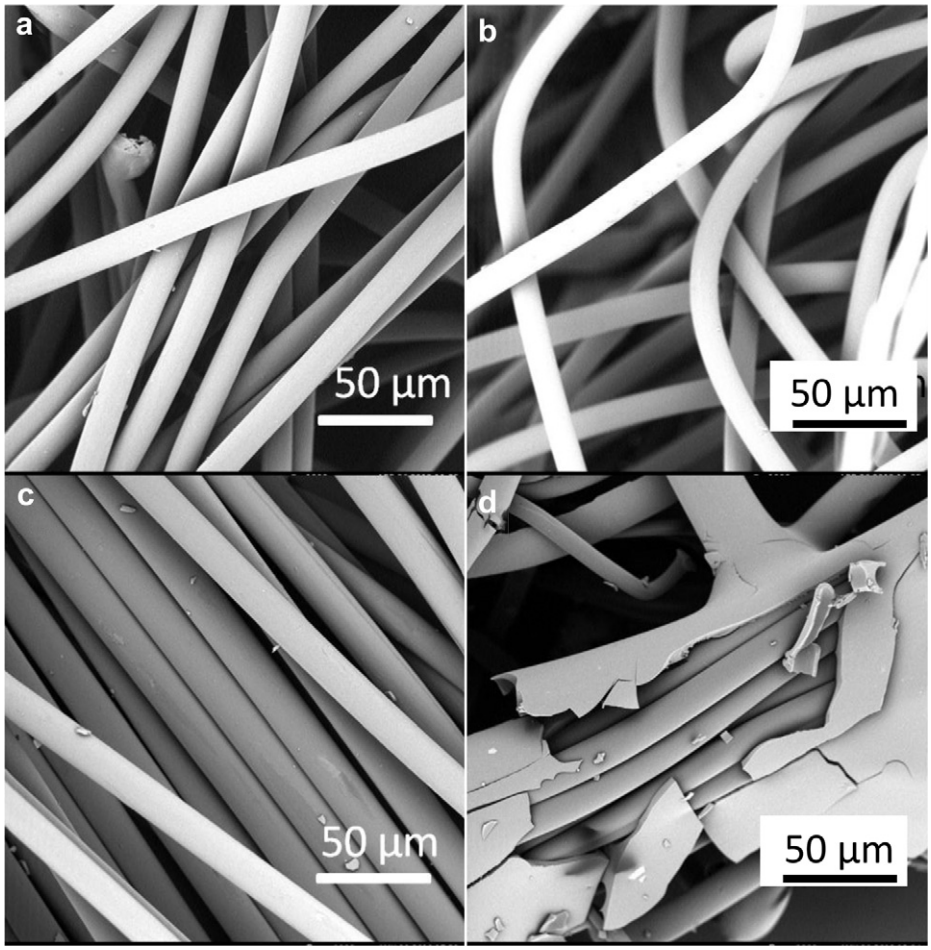

Fig. 1. Scanning electron microscope images collected from core/sheath bi-component fibers. Image (a) and (b) are form untreated PLA/PP and PP/PLA core/sheath fibers, respectively. Image (c) shows coated PLA/PP core/sheath fibers after 100 short ALD cycles, and the morphology is indistinguishable from the untreated fibers image (d) is collected from 100 short ALD coated PP/PLA core/sheath fibers. The PLA sheath appears to have flowed and blended together with adjacent fibers resulting in a cracked and nonuniform coating. However, the inner PP core remain intact and are readily visible after treatment.

formation of aluminum carbonate. A differential spectrum after the water pulse shows a decrease in the O–C–O stretching mode, consistent with aluminum carbonate hydroxylation. Fig. 2b shows in-situ FTIR analysis of TMA/water exposure on a PP film. The bottom spectrum is from the PP, and the other spectra show the absorbance change upon exposure to TMA or water. No change occurs upon exposure to TMA, or after the next water step, consistent with the inert structure of the polypropylene [23].

We also used XPS to examine TMA/water treated PLA films before and after a long exposure sequence at 120 °C. Fig. 3 shows XPS results before and after TMA infiltration. The survey scans show an increase in aluminum and oxygen. The C 1s peak near

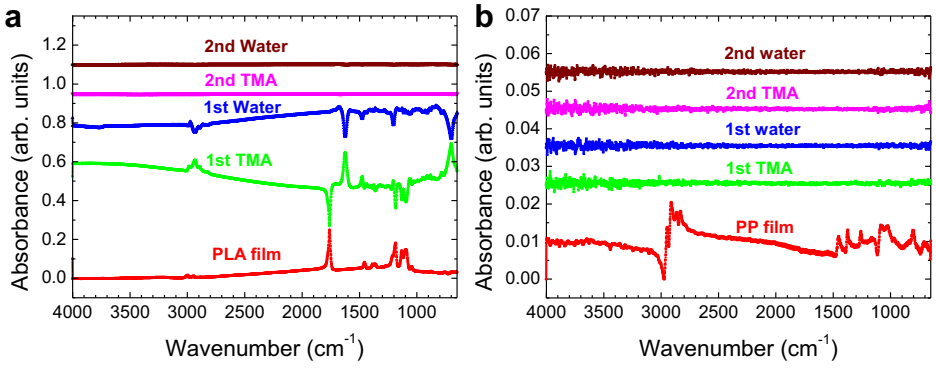

Fig. 2. In-situ FTIR spectra collected during the first two "long" TMA/water ALD cycles on single component PLA and PP films. Panel (a) shows the IR spectra collected from PLA, and (b) shows corresponding results from PP film. The bottom spectrum is from the untreated PLA or PP film on a Si wafer. The spectra, from bottom to top, correspond to differential spectra collected after each reagent exposure step. The data in (a) shows significant reaction between TMA and the carbonyl groups in PLA, whereas panel (b) indicates negligible reaction between TMA and PP.

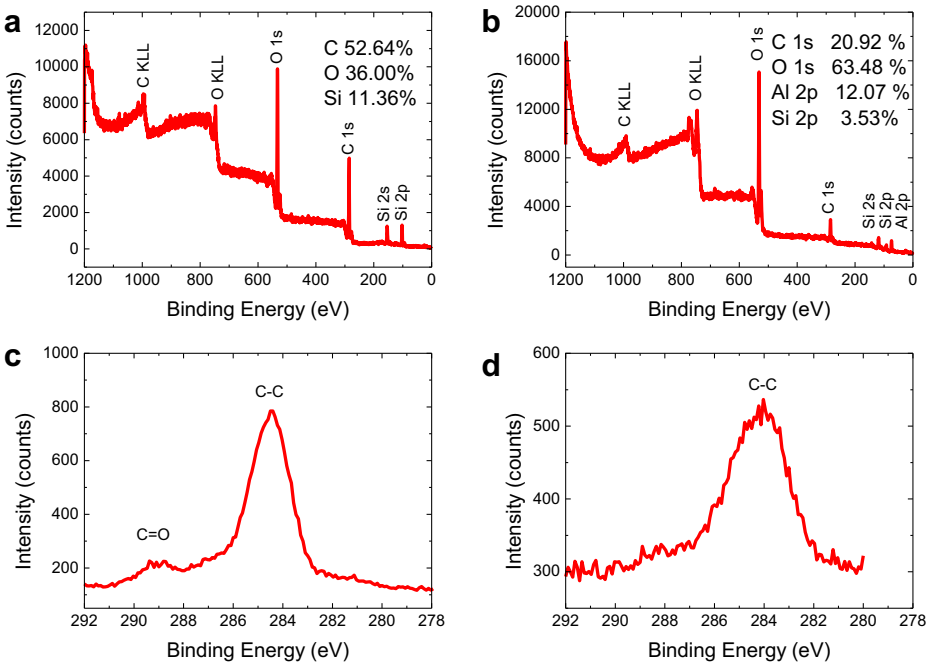

Fig. 3. XPS spectra collected from the PLA film on Si wafer: (a) and (b) untreated PLA; (c) and (d) PLA after one "long" TMA/water exposure cycle. The TMA exposure results in significant Al uptake (12 atomic %). The detailed C 1s scan for untreated PLA (panel c) shows peaks at 284.5 eV (C–C) and 289 eV (C=O), but after one "long" TMA/water exposure the peak at 289 eV is removed (panel d), indicating TMA reaction with carbonyl groups in the PLA.

289 eV present in the PLA is significantly reduced after TMA/water exposure, consistent with TMA reacting with C=O groups. XPS survey spectra collected on PP films after TMA/water exposure (not shown) indicated no detectable aluminum.

Fig. 4 shows TEM images collected from the untreated and ALD treated PLA/PP fibers. Panel (b) was collected after 500 short ALD cycles, and panel (c) shows the structure after 100 long ALD cycles at 120 °C. The core/sheath structure remains intact after ALD. The dark dots in the PP sheath in panel (a) are impurities present in the source polymer. After 500 short ALD cycles, image (b) shows a dark conformal aluminum oxide coating on outside PP layer [22,23,34]. The TEM image also shows particles in the PP near the interface, consistent with some diffusion of TMA into the PP layer [22,23]. The structure after 100 long ALD cycles is clearly different. Only a very thin, if any, conformal coating is present. The PP shell has a graded contrast with a darker region near the outer edge, consistent with particles in the near surface region [22,23] and the PLA core shows a striking two-layer structure, consistent with a diffusion limited reaction into the PLA.

Energy-dispersive X-ray spectroscopy data in Fig. 5 confirm that TMA can diffuse through the PP sheath and react with the PLA core. After 500 short cycles at 120 °C, the untreated PP/PLA core/sheath fiber shows no detectable aluminum. The Al is limited to a thin outer coating. However, after 100 long ALD cycles, the Al is much more distributed through the PP and PLA. It is interesting to note that there is an enrichment of Al at the outer edge of both the PP and PLA. Fig. 6 shows a schematic of TMA selective infusion and reaction on a PLA/PP core/sheath fiber. For short TMA/water doses, the precursor does not have sufficient time to diffuse deep into the PP layer and get to the PLA. This leads, after several ALD cycles, to a thin conformal Al_2O_3 layer on the outer PP surface, with some particles and oxide clusters within the PP near surface region. On the other hand, the "long" precursor exposure enhances the TMA and water vapor diffusion through the PP layer, where it readily

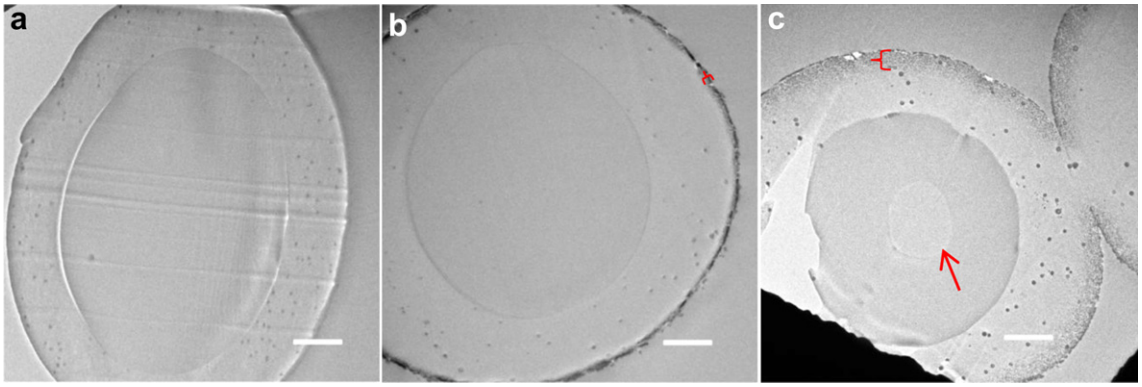

Fig. 4. The cross-sectional TEM images of epoxy-embedded: (a) untreated PLA/PP core/sheath fiber; (b) PLA/PP core/sheath fiber after 500 "short" TMA/water ALD cycles; and (c) PLA/PP core/sheath fiber after 100 "long" TMA/water cycles. The "short" ALD cycles lead to a thin Al_2O_3 film on the outer PP, with some sub-surface particles. In comparison, 100 "long" cycles lead to sharp contrast in the inner PLA core.

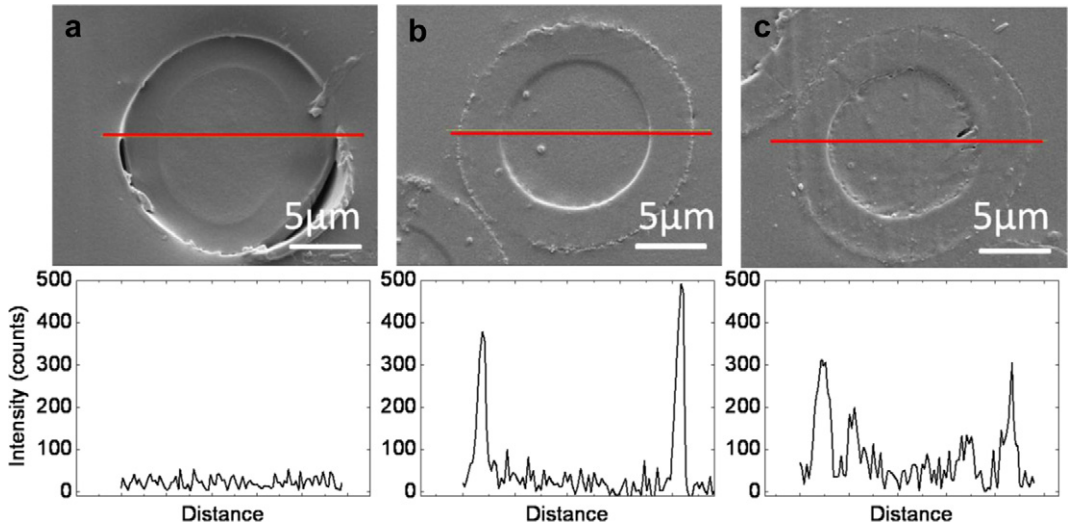

Fig. 5. Cross-sectional SEM images and EDS line scans collected from PLA/PP core/sheath fibers: (a) untreated; (b) after 500 "short" ALD cycles; and (c) after 100 "long" exposure cycles. For the untreated fiber, the EDS line scan along the fiber diameter shows no detectable Al. The "short" cycles produce Al on the outer edge of the PP with negligible Al in the PLA, whereas the long cycles lead to Al on the outer edge of the PP as well as distributed within the PLA core.

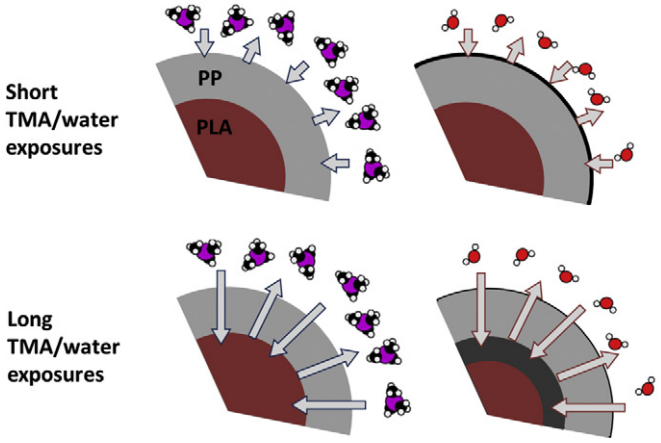

Fig. 6. Schematic diagram showing results of the "short" and "long" TMA/water ALD cycles on PLA/PP core/sheath bi-component fibers. The "short" TMA/water exposures minimize the time available for reactant diffusion, leading to a thin Al_2O_3 ALD layer on the PP surface. The "long" exposures permit TMA and water to diffuse through the PP and react with the PLA core.

reacts with the PLA core. While the TMA/water sequence may yield some solid oxide clusters within the PP shell, the TEM image (Fig. 4c) shows a marked contrast region the outer region of the PLA core, consistent with a mixed metal oxide/polymer layer surrounding an inner core polymer. These experiments were done at constant temperature. The substrate temperature can further control the extent of precursor diffusion and reaction [22,23]. Using this diffusion and reaction selectivity, more complex and pre-designed polymer/inorganic nanocomposite structures could be achieved formed in fibers or other media using judicious choice of reactants and reaction conditions.

4. Summary

Aluminum oxide films and particles can be selectively distributed into core/sheath bi-component fibers by controlling vapor exposure times and conditions during atomic layer deposition. For long exposures, trimethylaluminum diffuses easily through a PP fiber shell to nucleate alumina on the PLA core. Short exposure times trap TMA at the PP surface, producing a conformal coating on the outer PP layer. In contrast, PLA shows high reactivity towards TMA vapor, with substantially more sub-surface reaction during long exposures. TEM, EDS, FTIR and XPS show consistent data. The difference in reactivity towards metal organic vapors enabled selective incorporation of aluminum oxide films and particles within different regions of bi-component PP/PLA and PLA/PP core/sheath fibers. This ALD-based selective polymer modification can be extended to a wide range of multi-component polymer systems to make many unique polymer/inorganic nanocomposite structures.

Acknowledgment

This work was supported by the National Science Foundation project number CBET-1034374.

References

[1] Mal NK, Fujiwara M, Tanaka Y. Photocontrolled reversible release of guest molecules from coumarin-modified mesoporous silica. Nature 2003;421:350.
[2] Sershen SR, Westcott SL, Halas NJ, West JL. Temperature-sensitive polymer-nanoshell composites for photothermally modulated drug delivery. Journal of Biomedical Materials Research 2000;51:293.
[3] Feng XS, Huang RYM. Liquid separation by membrane pervaporation: a review. Industrial & Engineering Chemistry Research 1997;36:1048.
[4] Moore TT, Koros WJ. Non-ideal effects in organic-inorganic materials for gas separation membranes. Journal of Molecular Structure 2005;739:87.
[5] Moore TT, Mahajan R, Vu DQ, Koros WJ. Hybrid membrane materials comprising organic polymers with rigid dispersed phases. Aiche Journal 2004; 50:311.
[6] Gomez-Romero P. Hybrid organic-inorganic materials — in search of synergic activity. Advanced Materials 2001;13:163.
[7] Kamat PV. Meeting the clean energy demand: nanostructure architectures for solar energy conversion. Journal of Physical Chemistry C 2007;111:2834.
[8] Law M, Greene LE, Johnson JC, Saykally R, Yang PD. Nanowire dye-sensitized solar cells. Nature Materials 2005;4:455.
[9] Rosi NL, Eckert J, Eddaoudi M, Vodak DT, Kim J, O'Keeffe M, et al. Hydrogen storage in microporous metal-organic frameworks. Science 2003;300:1127.
[10] Sun DF, Ma SQ, Ke YX, Collins DJ, Zhou HC. An interweaving MOF with high hydrogen uptake. Journal of the American Chemical Society 2006;128:3896.
[11] Gangopadhyay R, De A. Conducting polymer nanocomposites: a brief overview. Chemistry of Materials 2000;12:608.
[12] Kashiwagi T, Grulke E, Hilding J, Groth K, Harris R, Butler K, et al. Thermal and flammability properties of polypropylene/carbon nanotube nanocomposites. Polymer 2004;45:4227.
[13] Pan YX, Yu ZZ, Ou YC, Hu GH. A new process of fabricating electrically conducting nylon 6/graphite nanocomposites via intercalation polymerization. Journal of Polymer Science Part B-Polymer Physics 2000;38:1626.

[14] Paul DR, Robeson LM. Polymer nanotechnology: nanocomposites. Polymer 2008;49:3187.
[15] Sanchez C, Ribot F. Design of hybrid organic-inorganic materials synthesized via sol-gel chemistry. New Journal of Chemistry 1994;18:1007.
[16] Kojima Y, Usuki A, Kawasumi M, Okada A, Fukushima Y, Kurauchi T, et al. Mechanical-properties of nylon 6-clay hybrid. Journal of Materials Research 1993;8:1185.
[17] LeBaron PC, Wang Z, Pinnavaia TJ. Polymer-layered silicate nanocomposites: an overview. Applied Clay Science 1999;15:11.
[18] Novak BM. Hybrid nanocomposite materials – between inorganic glasses and organic polymers. Advanced Materials 1993;5:422.
[19] Caruso RA, Susha A, Caruso F. Multilayered titania, silica, and laponite nanoparticle coatings on polystyrene colloidal templates and resulting inorganic hollow spheres. Chemistry of Materials 2001;13:400.
[20] Srivastava S, Kotov NA. Composite layer-by-layer (LBL) assembly with inorganic nanoparticles and nanowires. Accounts of Chemical Research 2008;41:1831.
[21] Gong B, Peng Q, Jur JS, Devine CK, Lee K, Parsons GN. Sequential vapor infiltration of metal oxides into sacrificial polyester fibers: shape replication and controlled porosity of microporous/mesoporous oxide monoliths. Chemistry of Materials 2011;23:3476.
[22] Jur JS, Spagnola JC, Lee K, Gong B, Peng Q, Parsons GN. Temperature-dependent subsurface growth during atomic layer deposition on polypropylene and cellulose fibers. Langmuir 2010;26:8239.
[23] Spagnola JC, Gong B, Arvidson SA, Jur JS, Khan SA, Parsons GN. Surface and sub-surface reactions during low temperature aluminium oxide atomic layer deposition on fiber-forming polymers. Journal of Materials Chemistry 2010; 20:4213.
[24] Peng Q, Tseng Y-C, Darling SB, Elam JW. Nanoscopic patterned materials with tunable dimensions via atomic layer deposition on block copolymers. Advanced Materials 2010;22:5129.
[25] Gong B, Parsons GN. Quantitative in-situ infrared analysis of reactions between trimethylaluminum and polymers during Al2O3 atomic layer deposition. Chemistry 2012;22:15672.
[26] Arvidson SA, Wong KC, Gorga RE, Khan SA. Structure, molecular orientation, and resultant mechanical properties in core/sheath poly(lactic acid)/polypropylene composites. Polymer 2012;53:791.
[27] Dorgan JR, Janzen J, Clayton MP, Hait SB, Knauss DM. Melt rheology of variable L-content poly(lactic acid). Journal of Rheology 2005;49:607.
[28] Peng Q, Gong B, VanGundy RM, Parsons GN. "Zincone" zinc oxide-organic hybrid polymer thin films formed by molecular layer deposition. Chemistry of Materials 2009;21:820.
[29] Gong B, Peng Q, Parsons GN. Conformal organic – inorganic hybrid network polymer thin films by molecular layer deposition using trimethylaluminum and glycidol. Journal of Physical Chemistry B 2011;115:5930.
[30] Jarvela P, Shucai L. Dynamic mechanical properties and morphology of polypropylene/maleated polypropylene blends. Journal of Applied Polymer Science 1996;62:813.
[31] Engelberg I, Kohn J. Physicomechanical properties of degradable polymers used in medical applications – a comparative-study. Biomaterials 1991;12: 292.
[32] Goldstein DN, McCormick JA, George SM. Al(2)O(3) atomic layer deposition with trimethylaluminum and ozone studied by in situ transmission FTIR spectroscopy and quadrupole mass spectrometry. Journal of Physical Chemistry C 2008;112:19530.
[33] Li M, Dai M, Chabal YJ. Atomic layer deposition of aluminum oxide on carboxylic acid-terminated self-assembled monolayers. Langmuir 2009;25: 1911.
[34] Hyde GK, Scarel G, Spagnola JC, Peng Q, Lee K, Gong B, et al. Atomic layer deposition and abrupt wetting transitions on nonwoven polypropylene and woven cotton fabrics. Langmuir 2009;26:2550.